Enhancing Thermoelectric Performance of $AgSbTe_2$ via Boron Doping and Composition Tuning

*Kivanc Saglik, Xizu Wang, Xian Yi Tan, Qiang Zhu, Ping Luo, Zhongzhen Luo, Jing Zhou, Dongwang Yang, Mingsheng Zhang, Qingyu Yan**

Kivanc Saglik

School of Materials Science and Engineering, Nanyang Technological University, 50 Nanyang Ave, Block N4.1, Singapore 639798, Republic of Singapore; Institute of Materials Research and Engineering (IMRE), Agency for Science, Technology, and Research (A*STAR), 2 Fusionopolis Way, Singapore 138634, Republic of Singapore

Xizu Wang

Institute of Materials Research and Engineering (IMRE), Agency for Science, Technology, and Research (A*STAR), 2 Fusionopolis Way, Singapore 138634, Republic of Singapore

Xian Yi Tan

School of Materials Science and Engineering, Nanyang Technological University, 50 Nanyang Ave, Block N4.1, Singapore 639798, Republic of Singapore; Institute of Materials Research and Engineering (IMRE), Agency for Science, Technology, and Research (A*STAR), 2 Fusionopolis Way, Singapore 138634, Republic of Singapore

Qiang Zhu

Institute of Materials Research and Engineering (IMRE), Agency for Science, Technology, and Research (A*STAR), 2 Fusionopolis Way, Singapore 138634, Republic of Singapore; Institute of Sustainability for Chemicals, Energy and Environment ($ISCE^2$), Agency for Science, Technology, and Research (A^*STAR), 1 Pesek Road, Jurong Island, 627833, Singapore

Ping Luo

Institute of Materials Research and Engineering (IMRE), Agency for Science, Technology, and Research (A*STAR), 2 Fusionopolis Way, Singapore 138634, Republic of Singapore

Zhongzhen Luo

Key Laboratory of Advanced Materials Technologies, International Joint Laboratory on Advanced Materials Technologies, College of Materials Science and Engineering, Fuzhou University, Fuzhou, 350108, P.R. China.

Jing Zhou

Key Laboratory of Advanced Materials Technologies, International Joint Laboratory on Advanced Materials Technologies, College of Materials Science and Engineering, Fuzhou University, Fuzhou, 350108, P.R. China.

Dongwang Yang

State Key Laboratory of Advanced Technology for Materials Synthesis and Processing, Wuhan University of Technology, Wuhan, 430070, China; School of Materials Science and Engineering,

Nanyang Technological University, 50 Nanyang Ave, Block N4.1, Singapore 639798, Republic of Singapore

Mingsheng Zhang

Institute of Materials Research and Engineering (IMRE), Agency for Science, Technology, and Research (A*STAR), 2 Fusionopolis Way, Singapore 138634, Republic of Singapore.

Qingyu Yan

School of Materials Science and Engineering, Nanyang Technological University, 50 Nanyang Ave, Block N4.1, Singapore 639798, Republic of Singapore;

E-mail: alexyan@ntu.edu.sg

* Corresponding author

KEYWORDS: thermoelectricity, chalcogenides, $AgSbTe_2$, boron, stoichiometry

ABSTRACT

Developing thermoelectric materials for medium-temperature applications is crucial for sustainable energy technologies. $AgSbTe_2$ is a promising material due to its intrinsically low thermal conductivity. However, its application is hindered by the n-type Ag_2Te impurities. In this study, we successfully suppressed Ag_2Te formation through B doping and composition modification. The suppression of Ag_2Te is confirmed by SEM and TEM studies, along with the linear temperature dependence of carrier concentration, electrical conductivity, and power factor, indicating a stable electronic transport behavior. Ag_2Te suppression enhanced carrier

concentration and electrical conductivity, leading to a temperature-independent power factor around 1.22 $mWm^{-1}K^{-2}$ between 300 and 625 K. Jonker plot analysis indicates that B doping and composition modulation improve intrinsic electronic properties. TEM and Debye-Callaway modeling further reveal that enhanced dislocations are responsible for the reduction in lattice thermal conductivity. Consequently, the figure of merit (zT) of the $Ag_{0.91}Sb_{1.09}Te_{2.09}$ + 0.025 wt% B sample increased to 1.35 at 573 K, while the average zT increased to 1.03. Compared to literature, this approach achieves one of the highest zT values reported through composition optimization and doping. These results highlight the potential of boron doping and composition tuning to enhance $AgSbTe_2$ as an efficient medium-temperature thermoelectric material.

INTRODUCTION

With the growing demand for clean energy resources, thermoelectric materials have gained increasing attention due to their intrinsic ability to directly convert heat into electricity.[1] The power conversion efficiency (PCE,η) of thermoelectric devices is determined by their thermoelectric figure of merit, zT, defined as $zT = (S^2\sigma\kappa^{-1})T$, where S, σ, κ, and T represent the Seebeck Coefficient, electrical conductivity, thermal conductivity, and temperature, respectively.[2] As the zT equation indicates, an ideal thermoelectric material should exhibit a high Seebeck coefficient (S) and electrical conductivity (σ), along with low thermal conductivity (κ). However, simultaneous optimization of these interdependent transport properties is challenging due to their mutual dependence on carrier concentration.[3] To overcome these limitations, several strategies have been developed to enhance thermoelectric performance. These include boosting the power factor through band engineering,[4, 5] optimizing carrier concentration,[6] and reducing the lattice thermal conductivity via defect engineering,[7] high-entropy approaches,[8, 9] and all-scale hierarchical microstructures.[10] These efforts have led to the discovery of several high-zT materials, such as

$AgMnGePbSbTe_5$,[9] SnSe,[11] GeTe,[12] Bi_2Te_3[13]-based compounds. Thanks to these advancements, thermoelectric materials now find applications in diverse fields, including automotive systems,[7] wearable electronics,[14] and space exploration.[2]

Among these materials, $AgSbTe_2$ stands out as a promising candidate for low-to-moderate temperature applications, owing to its intrinsically low thermal conductivity attributed to the $5s^2$ lone pairs of Sb,[15] similar to other Sb-containing materials such as Cu_3SbSe_3[16] and $CuSbSe_2$.[17] The thermal conductivity of $AgSbTe_2$ has been further reduced by introducing stacking faults,[15] and doping with Zn,[18] or Bi.[19] $AgSbTe_2$ also benefits from a decent Seebeck coefficient due to its highly degenerate electronic bands. However, the flatness of these bands results in low carrier mobility and electrical conductivity.[4, 20] Nevertheless, a carrier concentration around 10^{19} cm^{-3} helps keep a reasonably high power factor.

Early DFT studies on $AgSbTe_2$ suggest that transport is dominated by low-mobility holes and highly mobile electrons, which leads to a positive Seebeck coefficient but a negative Hall coefficient (R_H).[21] Structurally, $AgSbTe_2$ adopts a face-centered cubic lattice, with Ag and Sb atoms are randomly distributed over the cationic sublattice, resulting in atomic disorder that significantly affects the electronic transport properties.[22] For instance, increased disorder shifts the mobility edge closer to the Fermi level, thereby reducing electrical conductivity while increasing the Seebeck coefficient.[23] Fine-tuning of this disorder is therefore crucial for optimizing the power factor. Cd doping, for example, has been shown to reduce atomic disorder, enhance power factor, and suppress lattice thermal conductivity.[24] Additional strategies to enhance the power factor include Sn doping for band engineering,[25] equilibrium slow cooling to increase carrier concentration,[26] and Ti doping.[27]

However, $AgSbTe_2$ suffers from phase instability due to the formation of Ag_2Te, an inevitable secondary phase stemming from the small energy difference between $AgSbTe_2$ and a mixture of Ag_2Te and Sb_2Te_3.[23] The electromigration in $AgSbTe_2$ results in Ag_2Te precipitates with high electrical resistivity, which compromises long term stability. Notably, Ag_2Te is an n-type thermoelectric material that undergoes a phase transition near 418 K, further deteriorating thermoelectric performance.[23, 28] Consequently, numerous studies have aimed to suppress Ag_2Te formation via doping,[24] compositional optimization,[29] or annealing-quenching treatments.[28] Nevertheless, a small, stable amount of Ag_2Te is not necessarily detrimental and can be tolerated if its content remains constant over time.[28, 30]

Among potential dopants, boron stands out due to its high natural abundance, low toxicity, and intrinsically low thermal conductivity. It has been successfully incorporated into various p-type thermoelectric materials, such as $Bi_{0.5}Sb_{1.5}Te_3$ and Cu_2Se, where it helps tune electrical properties and reduce lattice thermal conductivity through enhanced grain boundary scattering.[31]

In this study, we first doped $AgSbTe_2$ with different amounts of boron (0.02, 0.025, and 0.03 wt%) to reduce lattice thermal conductivity. An optimized composition achieved a high zT of 1.23 through enhanced power factor and reduced lattice thermal conductivity. Subsequently, we adjusted the stoichiometry to $Ag_{0.91}Sb_{1.09}Te_{2.09}$ – within the stable composition range ($Ag_{1-x}Sb_{1+x}Te_{2+x}$) as indicated by phase diagrams[32] – and doped it with 0.025 wt% boron. All samples were synthesized using high-energy ball milling followed by moderate temperature heat treatment at 823 K, avoiding more energy intensive techniques like quenching or high-temperature annealing.[21, 33]

The combined strategy of boron doping and composition tuning enhanced the carrier concentration (n), effective mass (m^*), carrier mobilities (μ_W, μ_H, and μ_0), and electronic transport

coefficient (σ_{E0}), leading to improved electrical conductivity (σ) and power factor ($S^2\sigma$) of $Ag_{0.91}Sb_{1.09}Te_{2.09}$ + 0.025 wt% B. The power factor of this composition exhibits a high and stable value of 1.22 $Wm^{-1}K^2$ between 300 – 625 K, due to material homogeneity achieved by ball-milling synthesis. Debye-Callaway model and TEM analyses confirmed that the reduced thermal conductivity originates from dislocations and additional point defects. As a result, the average zT was increased to 1.03, compared to 0.65 in pristine $AgSbTe_2$, while the peak zT reached to 1.35. Single parabolic band (SPB) model suggests that zT values as high at 1.65 could be achieved through further optimization of the Fermi level and reduction of lattice thermal conductivity. This work thus demonstrates the boron doping and compositional modulation are effective strategies for enhancing thermoelectric performance and may be broadly applicable in the development of sustainable energy materials.

EXPERIMENTAL

The nominal compositions of $AgSbTe_2$ + x wt% B (x = 0.02, 0.025, and 0.03), $Ag_{0.91}Sb_{1.09}Te_{2.09}$, and $Ag_{0.91}Sb_{1.09}Te_{2.09}$ + 0.025 wt% B were prepared by weighing pure elements in an argon-filled glovebox. The elements were then loaded into stainless steel ball milling jars and milled for 90 minutes using a SPEX Sample Prep 8000M mill. The resulting powders were transferred into quartz ampoules, sealed under vacuum < 10^{-3} Pa, heated to 823 K over 5 hours, held at that temperature for 48 hours, and then allowed to cool naturally to room temperature. For thermoelectric performance measurements, the powders were consolidated using spark plasma sintering (SPX 211Lx, Fuji Electronic Industrial Co., Ltd., Japan) at 683 K under a uniaxial pressure of 60 MPa. Thermal diffusivity was measured using a Discovery Laser Flash 1200 system. Thermal conductivity was calculated as: $\kappa = D \times C_p \times \rho$, where D is the thermal diffusivity, C_p is the Dulong-Petit heat capacity, and ρ is the Archimedes density. Electrical resistivity and

Seebeck coefficient measurements were performed using the four-probe method with a ZEM-3 (Ulvac Riko). The estimated measurement uncertainties are ±3% for Seebeck coefficient, ±5% for electrical conductivity, ±7% for thermal conductivity and power factor, and ±10% for the figure of merit (zT).[34]

Phase identification was carried out by X-Ray diffraction (XRD) using a Bruker D8 Advance diffractometer with Cu-K_α radiation over a 2θ range of 10°-80°, with a step size of 0.02°. Microstructural characterization was performed using a field emission scanning electron microscope (FESEM, JEOL JSM-7600F) equipped with an energy-dispersive X-ray spectroscopy (EDS) detector. Transmission electron microscopy (TEM, JEOL JEM-2100F, Japan) was used for further microstructural analysis. Carrier concentration (n_H) and mobility (μ_H) were determined using the Van der Pauw method with an NYMS measurement system. Single-leg thermoelectric device performance was evaluated at Wuhan University of Technology using the PEM-1 setup (Ulvac, Japan)

RESULTS AND DISCUSSION

For simplicity, the samples are denoted as follows $AgSbTe_2$ → AST, $AgSbTe_2$ + 0.02 wt % B → AST + 0.02, $AgSbTe_2$ + 0.025 wt% B → AST + 0.025, $AgSbTe_2$ + 0.03 wt% B → AST + 0.03, $Ag_{0.91}Sb_{1.09}Te_{2.09}$ → NS – AST, and $Ag_{0.91}Sb_{1.09}Te_{2.09}$ + 0.025 wt% B → NS – AST + 0.025 in the figures.

Structural Characterization

The phase purity of $AgSbTe_2$ (AST), AST + 0.02, AST + 0.025, AST + 0.03, and $Ag_{0.91}Sb_{1.09}Te_{2.09}$ + 0.025 wt% B were analyzed by X – ray diffraction (XRD), as shown in Figure 1a. All samples were successfully indexed to the cubic $AgSbTe_2$ phase (Fm3m) along with minor monoclinic Ag_2Te impurities, which are known to be inevitable during $AgSbTe_2$ synthesis.[28] As

shown in Figure 1a(i), the most intense diffraction peak shifts to lower angles with increasing boron content up to 0.025 wt%, suggesting lattice expansion. However, with further boron doping (0.03 wt%) and in and $Ag_{0.91}Sb_{1.09}Te_{2.09}$ + 0.025 wt% B, the peak shift back toward higher angles, indicating a reversal in the trend. These observations are further corroborated by Rietveld refinement. Figure 1b reveals subtle variations in the lattice parameter (a=b=c) increasing slightly from 6.07 Å in pristine $AgSbTe_2$ to 6.08 Å in $Ag_{0.91}Sb_{1.09}Te_2$ + 0.025 wt% B. The overall changes in lattice parameters are minimal and consistent with previous reports,[29, 35] indicating that boron incorporation does not significantly alter the crystal structure. This outcome aligns with expectations based on the Hume-Rothery rules, considering the substantial ionic radius mismatch between B^{3+} (0.23 Å) and Ag^{+} (1.15 Å), Sb^{3+} (0.76 Å).

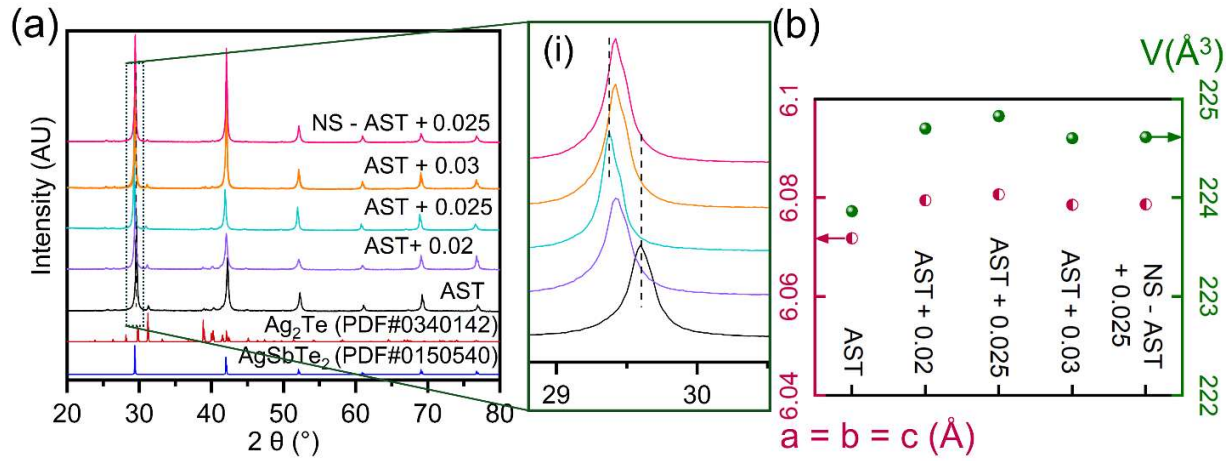

Figure 1. (a) XRD patterns, (i) zoomed- in diffractogram spanning from 2θ = 29 – 30.5°, (b) Lattice parameters and volume of $AgSbTe_2$ (AST), $AgSbTe_2$ + 0.02 wt% B (AST + 0.02), $AgSbTe_2$ + 0.025 wt% B, (AST + 0.025), $AgSbTe_2$ + 0.03 wt% B (AST + 0.03), $Ag_{0.91}Sb_{1.09}Te_{2.09}$ + 0.025 wt% B (NS – AST + 0.025).The Ag_2Te and $AgSbTe_2$ refer to theoretical XRD patterns with their PDF numbers provided in parantheses.

The microstructures of $AgSbTe_2$ + 0.025 wt% B and $Ag_{0.91}Sb_{1.09}Te_2$ + 0.025 wt% B were examined by scanning electron microscopy (SEM), as shown in Figures 2a and e, respectively. Elemental distribution maps of pristine $AgSbTe_2$ + 0.025 wt% B (Figures 2b-d) reveal two distinct regions: Ag-rich and Sb-rich. In all Ag-rich regions (Figure 2b) and Sb-rich regions, the elemental distributions are fully complementary. This suggests that Ag and Sb exhibit split-phase behavior across both regions. Additionally, Te appears similar to Sb but with a lighter contrast, indicating that Te and Sb are uniformly distributed and together form a continuous phase that is distinct from the Ag-rich phase, similar to other reports in the literature.[36] This microstructural separation represents a significant contrast to $Ag_{0.91}Sb_{1.09}Te_2$ + 0.025 wt% B (Figure 2e-h), where the elements are more homogeneously mixed. These results suggest that the formation of Ag_2Te precipitates is suppressed through the combined effects of boron doping and compositional tuning.

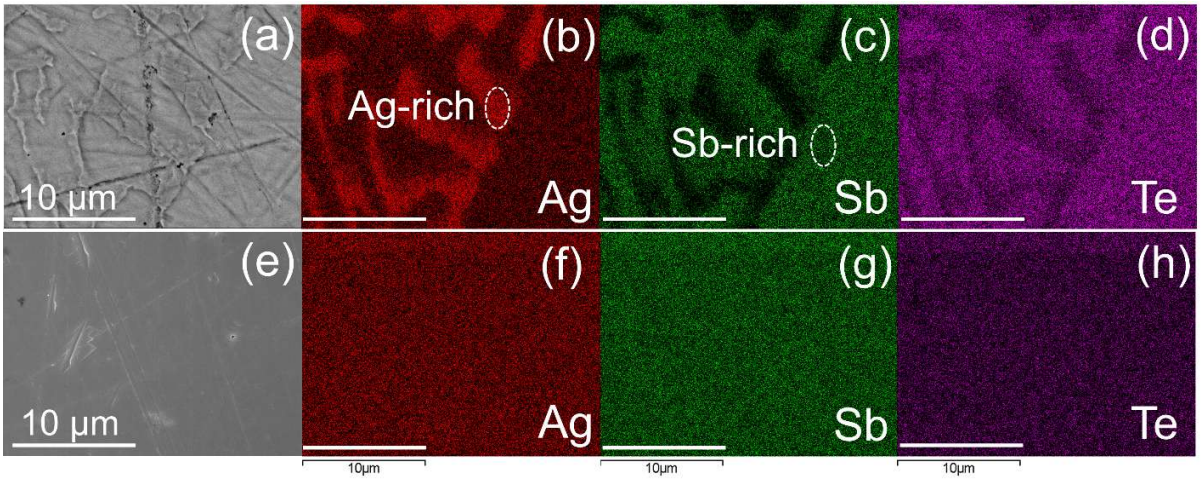

Figure 2. SEM EDS analysis of (a) – (d): $AgSbTe_2$ + 0.025 wt% B, and (e) – (h): $Ag_{0.91}Sb_{1.09}Te_{2.09}$ + 0.025 wt% B. Elemental maps showing the distribution of (b) & (d): Ag, (c) & (g): Sb, (d) & (h): Te

Electronic Transport Properties

The electronic transport properties of $AgSbTe_2$ + x wt% B and $Ag_{0.91}Sb_{1.09}Te_2$ + x wt% B are presented in Figure 3. The electrical conductivity of boron-doped $AgSbTe_2$ (AST + x wt% B) samples initially decreases with temperature up to ~450 K, characteristic of a degenerate semiconductor where carrier scattering increases with temperature. Beyond this point, the electrical conductivity begins to rise due to the activation of minority carriers, consistent with the narrow band gap nature of $AgSbTe_2$.[37] However, this bipolar conduction behavior appears to be suppressed in the compositionally optimized sample, $Ag_{0.91}Sb_{1.09}Te_{2.09}$ and $Ag_{0.91}Sb_{1.09}Te_{2.09}$ + 0.025 wt% B.

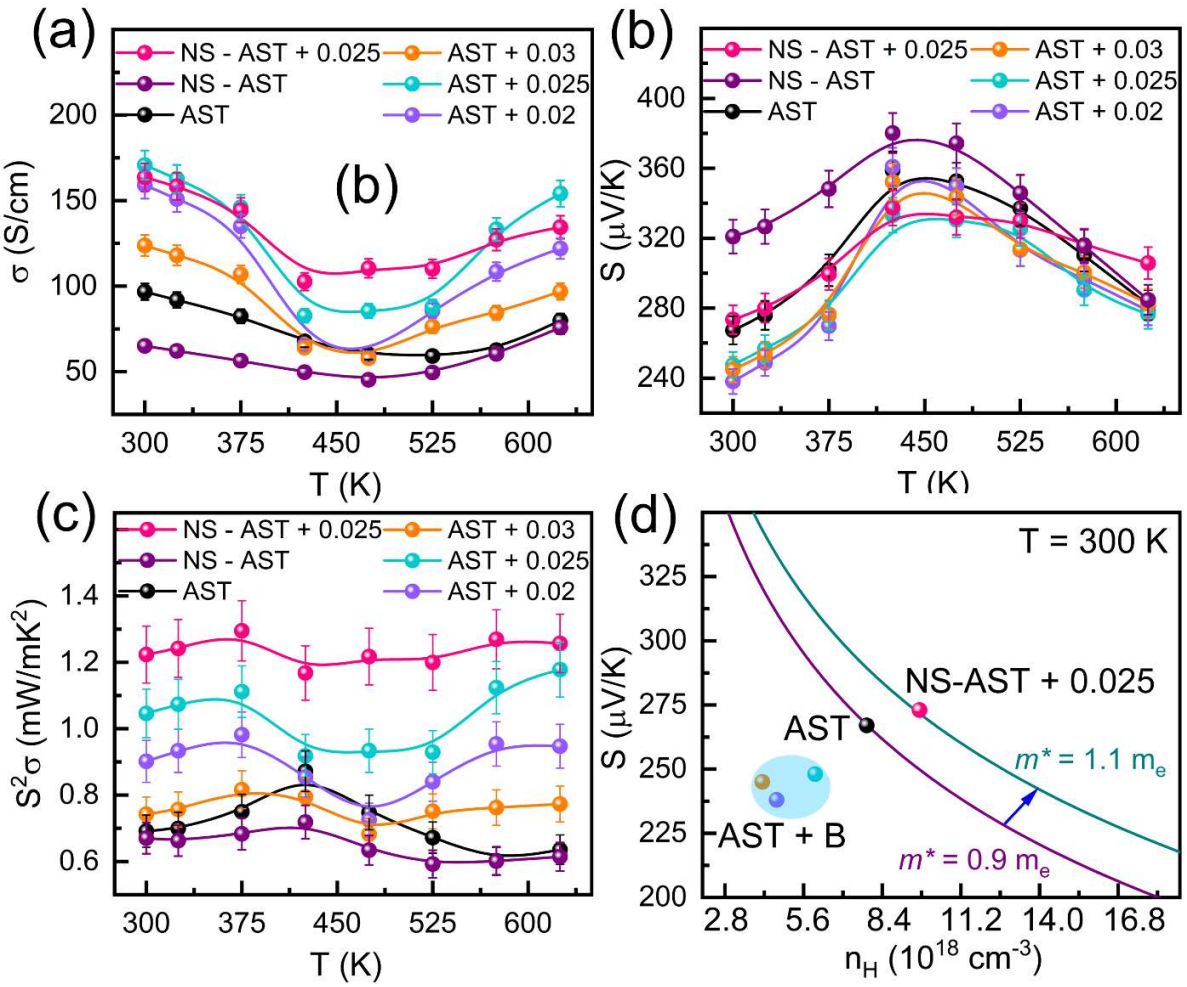

Figure 3 (a) Electrical conductivity, (b) Seebeck coefficient, (c) Power factor of $AgSbTe_2$ + x wt% B and $Ag_{0.91}Sb_{1.09}Te_{2.09}$ + 0.025 wt% B, with respect to the temperature. (d) Pisarenko plot, revealing the carrier concentration and effective mass of $AgSbTe_2$ + x wt% B and $Ag_{0.91}Sb_{1.09}Te_{2.09}$ + 0.025 wt% B.

As shown in Figure 3b, all samples exhibit positive Seebeck coefficients, indicating that holes are the dominant charge carriers. The Seebeck coefficient increases with temperature initially, then decreases at higher temperatures due to the excitation of minority carries, which reduces the overall Seebeck coefficient value. The band gaps of samples were estimated using the relation $E_g = 2 \times e \times |S_{max}| \times T_{max}$, yielding values around 0.29 eV, which aligns well with previously reported experimental results.[38]

Figure 3a reveals that boron doping markedly enhances electrical conductivity. Pristine $AgSbTe_2$ exhibits a room-temperature electrical conductivity of 96.72 Scm^{-1}, which rises to 163.60 Scm^{-1} in $Ag_{0.91}Sb_{1.09}Te_{2.09}$ + 0.025 wt% B. On the other hand, compositionally tuned sample, $Ag_{0.91}Sb_{1.09}Te_{2.09}$ has a significantly lower electrical conductivity compared to $AgSbTe_2$ and $Ag_{0.91}Sb_{1.09}Te_{2.09}$ + 0.025 wt% B, supporting that boron doping has a substantial impact on the electrical conductivity. The Seebeck coefficient shows a modest increase from 267 μVK^{-1} in $AgSbTe_2$ to 278 μVK^{-1} in $Ag_{0.91}Sb_{1.09}Te_{2.09}$ + 0.025 wt% B. As a result of the substantial increase in electrical conductivity while maintaining a high Seebeck coefficient, all boron-doped samples exhibit enhanced power factor values, as shown in Figure 3c. At room temperature, the power factor increases from 0.69 $Wm^{-1}K^{-2}$ for pristine $AgSbTe_2$ to 1.05 $Wm^{-1}K^{-2}$ for 1.05 in $AgSbTe_2$ + 0.025 wt%, and further to 1.22 $Wm^{-1}K^{-2}$ for $Ag_{0.91}Sb_{1.09}Te_2$ + 0.025 wt% B. The power factor of undoped $AgSbTe_2$ exhibits a peak around 425 K, which is likely associated with the phase transition of Ag_2Te. In boron-doped samples, a broad plateau is observed between 425 K and 525

K, suggesting the combined effects of minority carrier excitation and phase transition dynamics. The power factor of compositionally tuned $Ag_{0.91}Sb_{1.09}Te_{2.09}$ has a low but temperature independent value, which indicates homogenous distribution triggered by composition control. Notably, $Ag_{0.91}Sb_{1.09}Te_2$ + 0.025 wt% B exhibits an elevated power factor compared to all other compositions. In addition, the power factor remains remarkably stable over a broad temperature range (300 – 623 K), achieving an average value of 1.22 $Wm^{-1}K^{-2}$, exceeding those reported for various $AgSbTe_2$-based systems.[21, 27, 30] This strong temperature stability of power factor is most likely related to the homogenous distribution material distribution in $Ag_{0.91}Sb_{1.09}Te_2$ + 0.025 wt% B, which is further supported by the uniform elemental maps in the SEM (Figure 2). As a conclusion, the stable nature of the power factor of compositionally tuned samples indicates an enhanced homogeneity in the $Ag_{0.91}Sb_{1.09}Te_{2.09}$ and $Ag_{0.91}Sb_{1.09}Te_{2.09}$ + 0.025 wt% B.

To evaluate the electrical transport properties, we measured Hall mobilities (μ_H) and carrier concentrations (n_H) of $AgSbTe_2$ + x wt% B doped and $Ag_{0.91}Sb_{1.09}Te_{2.09}$ + 0.025 wt% B doped samples using the single parabolic band (SPB) model. The SPB model assumes acoustic phonon scattering dominance and a single parabolic band, therefore, deviations may arise in systems with multiband contributions,[39] such as $AgSbTe_2$. Room-temperature electronic transport properties for all samples, including carrier concentration dependencies, are summarized in Table 1.

Table 1 Room temperature carrier concentration, electrical conductivity, effective mass, Hall mobility and drift mobility values of $AgSbTe_2$ + x wt% B and $Ag_{0.91}Sb_{1.09}Te_{2.09}$ samples.

Composition	n_H (cm^{-3})	σ (Scm^{-1})	S (μVK^{-1})	m^* (m_e)	μ_H ($cm^2V^{-1}s^{-1}$)	μ_0 ($cm^2V^{-1}s^{-1}$)
AST	$7.85x10^{18}$	96.72	267	0.90	113.2	137
AST + 0.02	$4.64x10^{18}$	159.10	238	0.48	133.1	157
AST + 0.025	$6.01x10^{18}$	170.75	248	0.65	118.1	143

AST + 0.03	4.13×10^{18}	123.77	245	0.48	138.9	165
NS-AST + 0.025	9.73×10^{18}	163.60	273	1.10	53.8	67

The Pisarenko plot (Figure 3d) indicates that non-stoichiometric $Ag_{0.91}Sb_{1.09}Te_{2.09}$ + 0.025 wt% B exhibits enhanced carrier concentration (n_H) and effective mass (m^*) compared to pristine $AgSbTe_2$, consistent with its improved electrical conductivity (σ) and maintained Seebeck coefficient (S). In contrast, boron-doped samples show reduced effective mass, correlating with their slightly diminished Seebeck coefficient. However, their decreased carrier concentration contradicts the observed rise in electrical conductivity. To resolve this discrepancy, we analyzed Hall mobilities (μ_H, Figure 4a), revealing increased hall mobility in stoichiometric doped samples (113.2 → 180 $cm^2V^{-1}s^{-1}$), compared to pristine $AgSbTe_2$, which compensates for lower carrier mobility and enhances electrical conductivity.

Notably, the $Ag_{0.91}Sb_{1.09}Te_{2.09}$ + 0.025 wt% B sample displays significantly reduced hall mobility (53.8 $cm^2V^{-1}s^{-1}$) despite higher electrical conductivity, suggesting alternative conduction mechanisms. Temperature dependent carrier concentration (n_H) (Figure 4c) shows that carrier concentration increases with temperature across all samples, indicative of non-degenerate semiconducting behavior. Concurrently, the hall mobility (μ_H) (Figure 4c) decreases with temperature but exhibits an anomalous upturn in pristine $AgSbTe_2$ at elevated temperatures, likely due to Ag_2Te secondary phase contributions. This upturn is suppressed in $Ag_{0.91}Sb_{1.09}Te_{2.09}$ + 0.025 wt% B, implying reduced Ag_2Te precipitates.

Room-temperature Hall coefficient (R_H) values (Figure 4d) further clarify this behavior. Negative R_H alongside positive Seebeck coefficient suggests bipolar conduction, with holes from p-type $AgSbTe_2$ and electrons from n-type Ag_2Te.[21] The diminished R_H in $Ag_{0.91}Sb_{1.09}Te_{2.09}$ + 0.025 wt% B supports reduced Ag_2Te content, aligning with its lower carrier mobility. Prior

studies report hole and electron mobilities in $AgSbTe_2$ as ~11 and ~ 2200 $cm^2V^{-1}S^{-1}$, respectively. [40] The stark hall mobility reduction in $Ag_{0.91}Sb_{1.09}Te_{2.09}$ + 0.025 wt% B further corroborates Ag_2Te suppression.

Given the negligible disparity between drift (μ_0) and Hall mobilities (μ_H), we applied the single parabolic band (SPB) model for Jonker analysis, intrinsic electronic transport (σ_{E0}), and Fermi level modelling. While the SPB model assumed acoustic phonon scattering dominance, potential multiband effects in $AgSbTe_2$-derived systems warrant future investigation.

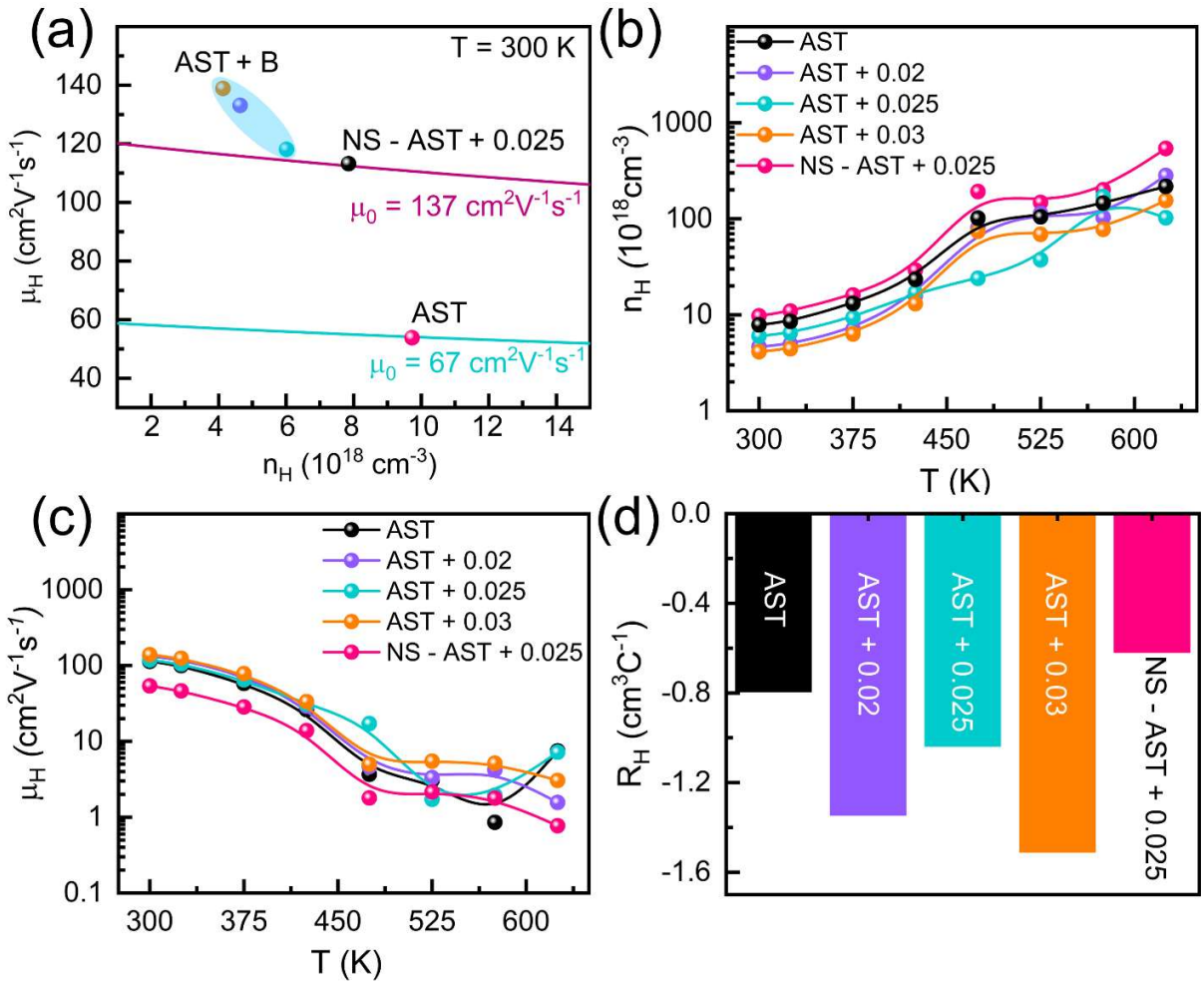

Figure 4 Temperature dependent (a) Hall carrier concentration, (b) Hall mobility of $AgSbTe_2$ + x wt% B and $Ag_{0.91}Sb_{1.09}Te_{2.09}$ + 0.025 wt% B, room temperature (c) Pisarenko plot that reveals the

effective mass, (d) simulated drift mobility of $AgSbTe_2$ + x wt% B and $Ag_{0.91}Sb_{1.09}Te_{2.09}$ + 0.025 wt% B.

To decouple the effects of carrier concentration and boron doping on intrinsic electronic properties, we analysed the weighted mobility (μ_W), electronic transport coefficient (σ_{E0}), Jonker plot, and quality factor (B) (Figure 5). Weighted mobility (μ_W) for $AgSbTe_2$ and stoichiometric boron-doped samples exhibits a pronounced hump near 400 K (Figure 5a), consistent with the cubic-to-monoclinic phase transition of $AgSbTe_2$.[41] This anomaly suggests additional scattering mechanism such as alloy or defect scattering beyond acoustic phonon-dominated scattering. In contrast, the $Ag_{0.91}Sb_{1.09}Te_{2.09}$ + 0.025 wt% B sample shows a linear temperature dependent weighted mobility, indicative of acoustic phonon scattering dominance. The absence of Ag_2Te secondary phases and increased atomic disorder in this sample, as supported by Hall coefficient trends (Figure 4d), eliminate phase-boundary scattering, enabling enhanced mobility and electrical conductivity.[25] Compositional tuning via non-stoichiometry and boron-doping in $Ag_{0.91}Sb_{1.09}Te_{2.09}$ + 0.025 wt% B suppresses defect scattering, shifting the dominant mechanism to acoustic phonon scattering. The resultant mobility increase directly correlates with improved electrical conductivity, even at reduced carrier concentrations. (Table 1)

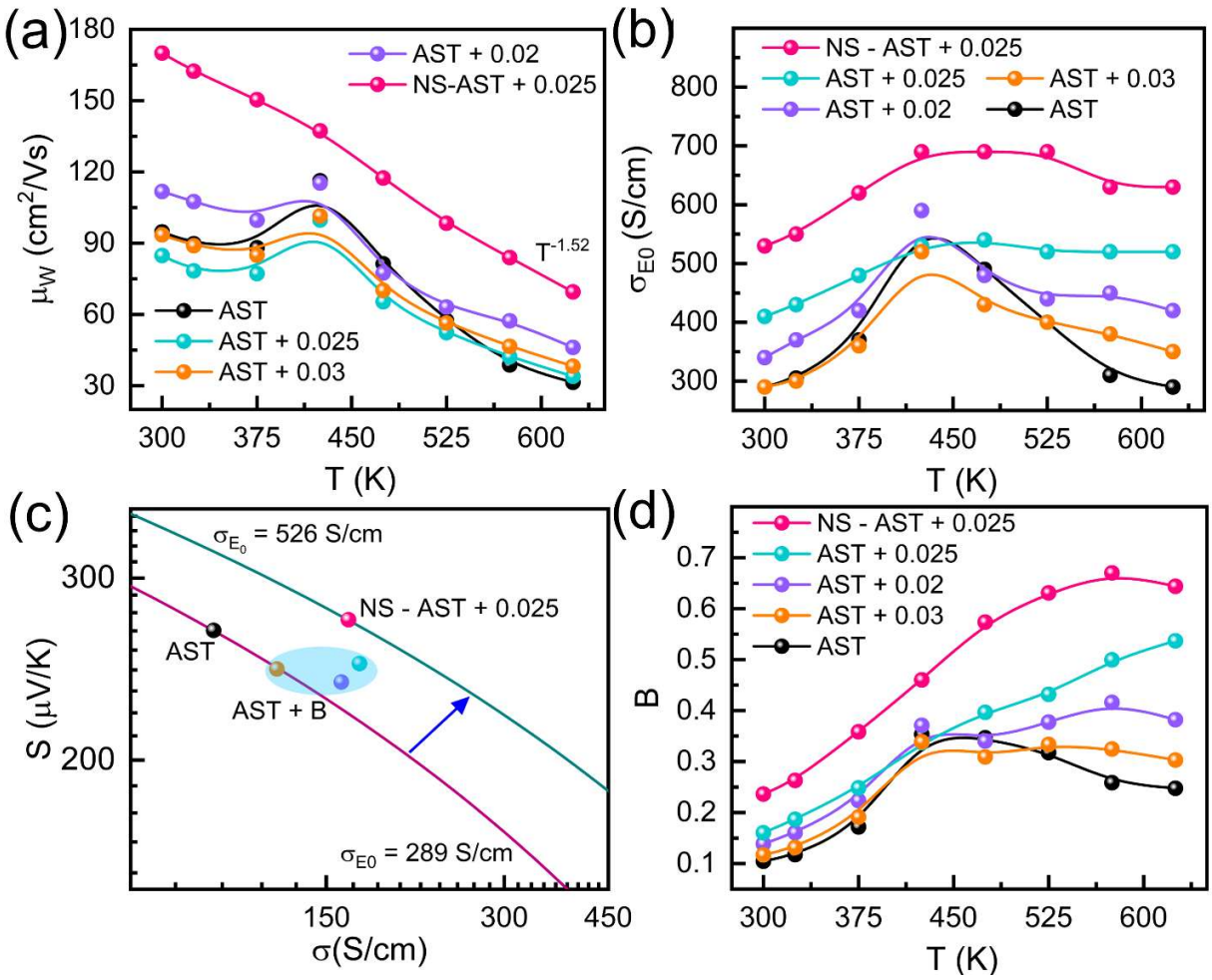

Figure 5 Temperature dependent (a) weighted mobility, (b) intrinsic transport coefficient, (d) quality factor, and (c) Jonker plot of $AgSbTe_2$ + x wt% B and $Ag_{0.91}Sb_{1.09}Te_{2.09}$ + 0.025 wt% B.

To further evaluate scattering mechanisms, we analyzed the intrinsic electronic transport coefficient across all samples (Figure 5b). Undoped $AgSbTe_2$ exhibits a pronounced hump in σ_{E0} near 425 K, indicative of mixed scattering mechanisms involving Ag_2Te phase transitions.[42] This anomaly diminishes in boron-doped stoichiometric samples, suggesting partial suppression of Ag_2Te-related scattering.[41] Notably, the non-stoichiometric $Ag_{0.91}Sb_{1.09}Te_{2.09}$ + 0.025 wt% B sample displays a nearly temperature-independent σ_{E0}, consistent with acoustic phonon scattering dominance and Ag_2Te suppression. Room temperature σ_{E0} values, plotted in the Jonker analysis

(Figure 5c), reveal that boron doping enhances σ_{E0} across all compositions. The optimized $Ag_{0.91}Sb_{1.09}Te_{2.09}$ + 0.025 wt% B sample achieves the highest σ_{E0}, demonstrating successful tuning of carrier scattering via boron-doping and stoichiometric control.[25]

The temperature-dependent quality factor (B) exhibits a marked improvement upon doping, as shown in Figure 5d. Specifically, the pristine $AgSbTe_2$ sample displays a B (quality factor) value of 0.26, which increases to 0.50 with the addition of 0.025 wt% B. Further enhancement is observed in the nonstoichiometric sample $Ag_{0.91}Sb_{1.09}Te_{2.09}$ + 0.025 wt% B, where B (quality factor) reaches 0.67. This progressive increase in B reflects the beneficial impact of boron doping and composition optimization on the electronic transport properties. The suppression of Ag_2Te precipitates in the nonstoichiometric samples is consistent with previous strategies for minimizing secondary-phase scattering in $AgSbTe_2$ systems, thereby contributing to improved electrical performance.[29]

Thermal Transport Properties

The total thermal conductivity of $AgSbTe_2$ + x wt% B and $Ag_{0.91}Sb_{1.09}Te_2$ + x wt% B is reported in Figure 4. Both boron doping and stoichiometry control lead to a reduction in the total thermal conductivity of $AgSbTe_2$, as shown in Figure 6a. Specifically, the total thermal conductivity of $AgSbTe_2$ decreases from 0.67 $Wm^{-1}K^{-1}$ in the pristine sample to 0.58 $Wm^{-1}K^{-1}$ in $Ag_{0.91}Sb_{1.09}Te_2$ + 0.025 wt% B at room temperature. The total thermal conductivity of $Ag_{0.91}Sb_{1.09}Te_{2.09}$ exhibits the lowest thermal conductivity, however, this composition cannot achieve an improved zT value, which will be explained later in this work. The thermal conductivity of all samples exhibits an upturn around 475 K, which suggests a bipolar contribution to the thermal conductivity at elevated temperatures. A similar trend is observed in the electronic thermal conductivity, where an upturn also occurs around 475 K, as shown in Figure 6b. The electronic thermal conductivities of all

samples follow the trend of their electrical conductivity (Figure 3a), which is expected due to the Lorenz relation, $\kappa_e=\sigma LT$. Since the electronic thermal conductivity of the boron-doped and stoichiometry-controlled samples increases, the observed reduction in total thermal conductivity can be attributed primarily to a significant reduction in the lattice thermal conductivity.

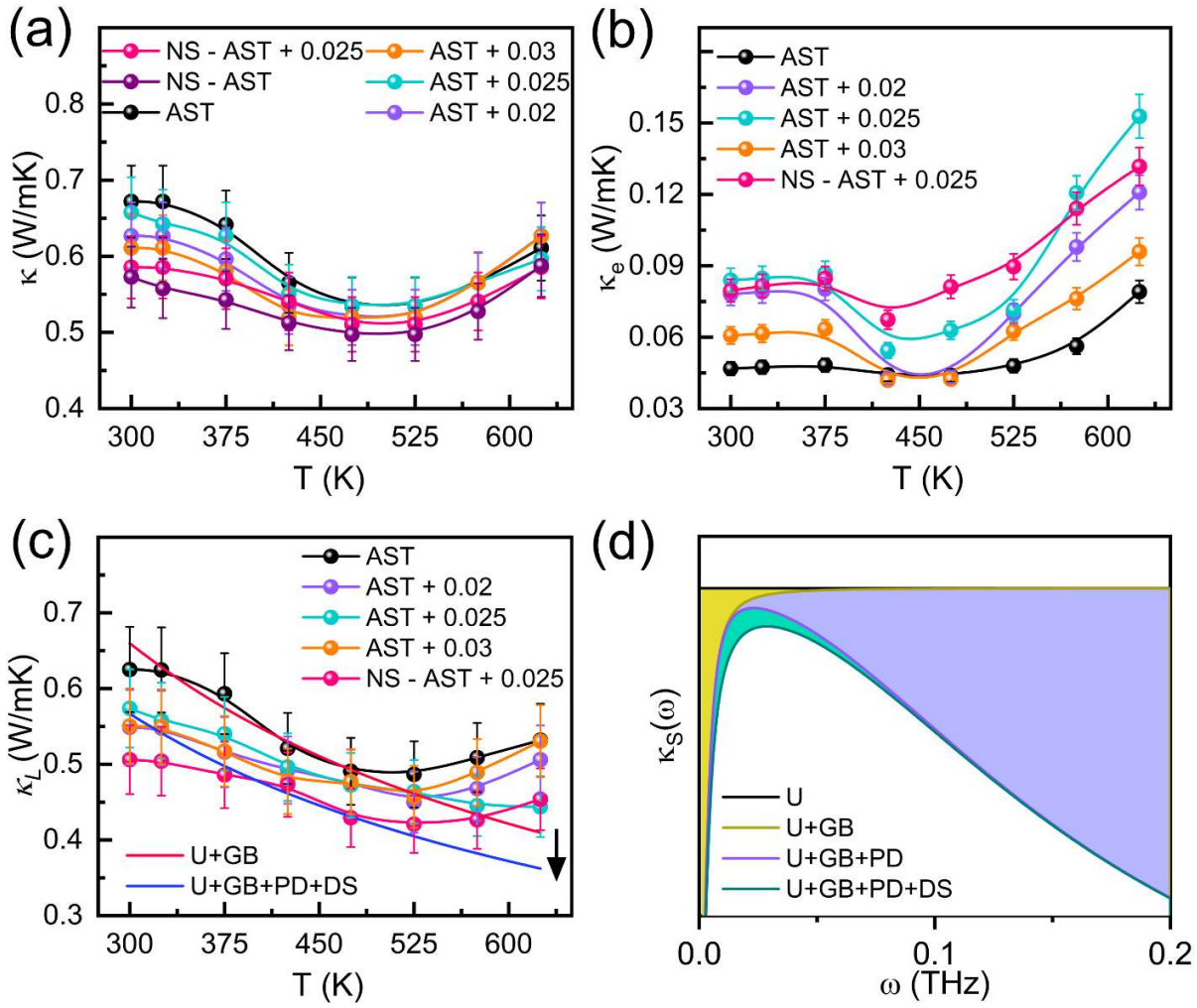

Figure 6 Temperature dependent (a) total, (b) electronic, (c) lattice thermal conductivity of $AgSbTe_2$ + x wt% B and $Ag_{0.91}Sb_{1.09}Te_{2.09}$ + 0.025 wt% B. (d) Spectral thermal conductivity showing Umklapp, point defect, grain boundary, and dislocation scattering for $Ag_{0.91}Sb_{1.09}Te_{2.09}$ + 0.025 wt% B.

To further investigate this, we analyzed the lattice thermal conductivity of the samples using the Debye-Callaway model. Figure 6c demonstrates that both boron doping and stoichiometry control reduce the lattice thermal conductivity in all samples. Notably, the lattice thermal conductivity of $Ag_{0.91}Sb_{1.09}Te_{2.09}$ + 0.025 wt% B is 0.50 $Wm^{-1}K^{-1}$, which is lower than that of the pristine $AgSbTe_2$ (0.62 $Wm^{-1}K^{-1}$). According to the Debye-Callaway model results presented in Figures 6c and d, point defect and dislocation scattering are the primary mechanisms responsible for the reduced lattice thermal conductivity in $Ag_{0.91}Sb_{1.09}Te_{2.09}$ + 0.025 wt% B, whereas the pristine sample is mainly affected by Umklapp scattering and grain boundary scattering.

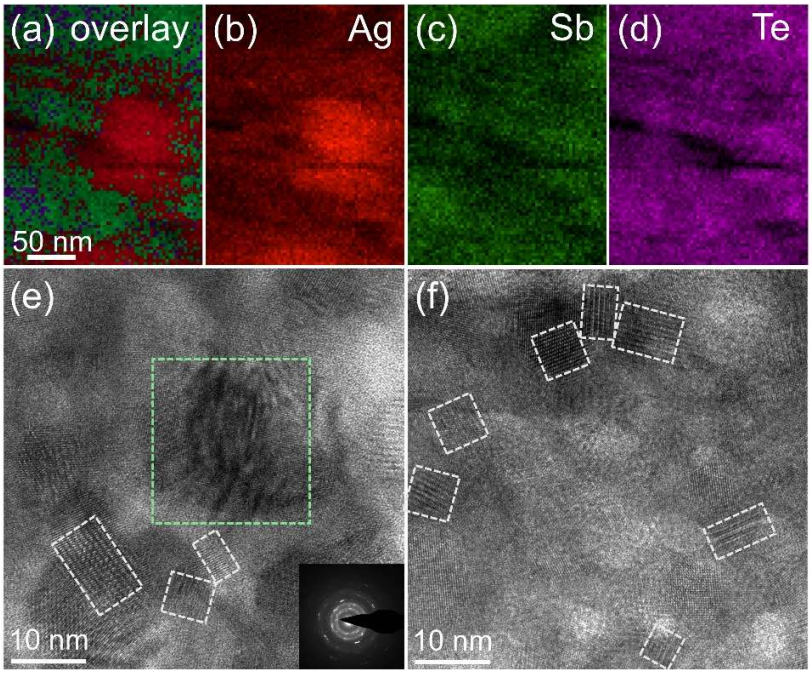

Figure 7 (a) TEM image of $Ag_{0.91}Sb_{1.09}Te_{2.09}$ + 0.025 wt% B showing the elemental distribution of (b) Ag, (c) Sb, and (d) Te. (e), (f) TEM images showing the nanoscale structures by white rectangles and ripple like lattices by the green rectangle. The inset image in (e) shows the SAED patterns.

To evaluate the impact of dislocation and point defect scattering mechanisms in $Ag_{0.91}Sb_{1.09}Te_{2.09}$ + 0.025 wt% B, we performed high-resolution transmission electron microscopy (HRTEM) analysis. The HRTEM image in Figure 7a, along with the elemental mapping images in Figure 7b, c, and d reveal the presence of Ag precipitates. Furthermore, Figures 7e and f show a high density of dislocations, which are likely to induce significant lattice strain. Consequently, the lattice thermal conductivity is effectively reduced, consistent with previous studies in the literature.[30] Additionally, the inset selected-area electron diffraction (SAED) image in Figure 7e indicates that the sample possesses a slightly polycrystalline nature, which can further reduce the lattice thermal conductivity due to increased scattering at grain boundaries.

Thermoelectric Performance

Figure 6 shows the thermoelectric figure of merit of $AgSbTe_2$ + x wt% B and $Ag_{0.91}Sb_{1.09}Te_{2.09}$ + 0.025 wt % B samples. Owing to enhanced and stable power factor along with reduced thermal conductivity, the peak zT of $Ag_{0.91}Sb_{1.09}Te_{2.09}$ + 0.025 wt% B increases to 1.35, representing a 121 % enhancement compared to the pristine sample. ($AgSbTe_2$, zT=0.61). Additionally, the zT values of all boron-doped samples exceed those of pristine $AgSbTe_2$ across the measured temperature range (300 – 625 K). Therefore, the average zT of pristine $AgSbTe_2$ increases from 0.56 to 1.03 in $Ag_{0.91}Sb_{1.09}Te_{2.09}$ + 0.025 wt % B. The peak and average zT values for $AgSbTe_2$ + x wt% B and $Ag_{0.91}Sb_{1.09}Te_{2.09}$ + 0.025 wt % B are summarized in Figure 8c and Figure 8d, respectively. The elevated peak and average zT values support that high homogeneity of $Ag_{0.91}Sb_{1.09}Te_{2.09}$ + 0.025 wt% B enhances the thermoelectric performance. On the other hand, pristine $Ag_{0.91}Sb_{1.09}Te_{2.09}$ has a lower zT compared to $Ag_{0.91}Sb_{1.09}Te_{2.09}$ + 0.025 wt% B, which underscores the impact of boron doping for enhancing the thermoelectric performance of both $AgSbTe_2$ and $Ag_{0.91}Sb_{1.09}Te_{2.09}$.

Additionally, the *zT* values of all samples were analyzed in relation to the Fermi level and quality factor using the Single Parabolic Band (SPB) model. As shown in Figure 8b, the Fermi level decreases with boron doping. However, in the compositionally tuned sample, $Ag_{0.91}Sb_{1.09}Te_{2.09}$ + 0.025 wt % B, the combined effect of composition adjustment and boron doping results in an increased Fermi level. This trend in the Fermi level is consistent with the variation in room-temperature carrier concentration among the samples, as listed in Table 1.

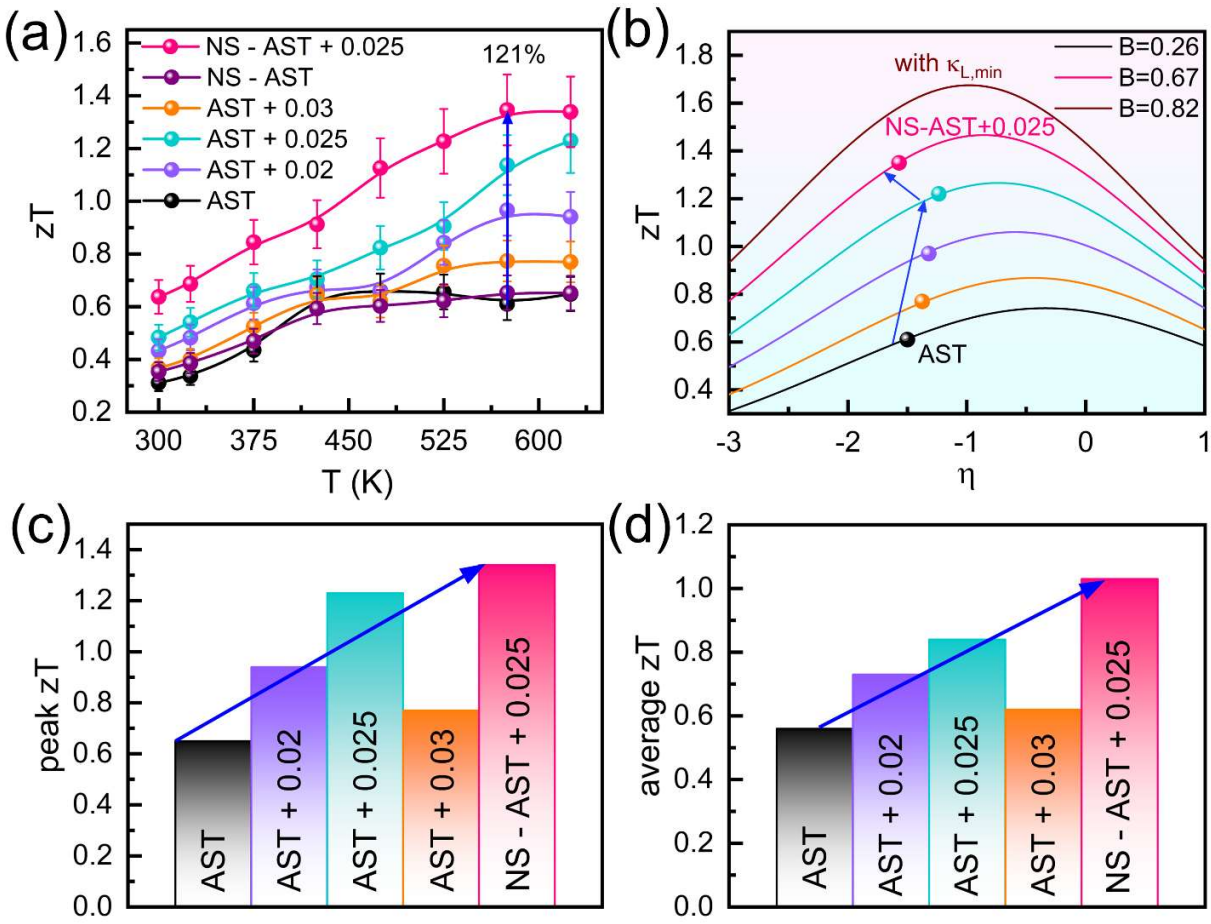

Figure 8 Temperature dependent thermoelectric figure of merit zT, (b) The relationship between zT, reduced Fermi level (η), and quality factor (B), (c) peak zT, and (d) average zT of $AgSbTe_2$ + x wt% B and $Ag_{0.91}Sb_{1.09}Te_{2.09}$ + 0.025 wt% B.

In addition, the quality factor of samples systematically increases with Boron doping and composition control, reaching a peak value of 0.67 in $Ag_{0.91}Sb_{1.09}Te_{2.09}$ + 0.025 wt% B. By fine-tuning the carrier concentration, the *zT* of this composition could be enhanced to 1.45. However, since the Fermi level is already close to optimal, a more effective strategy to improve the quality factor (and *zT*) would be to reduce the lattice thermal conductivity. The quality factor can be increased to 0.82 by lowering the lattice thermal conductivity to its theoretical minimum of 0.36 $Wm^{-1}K^{-1}$, as calculated by the Debye-Cahill model. As a result, the peak *zT* of this composition could reach as high as 1.65. Such a high *zT* may be achieved by adopting strategies that reduce thermal conductivity without adversely affecting electrical conductivity. For instance, the scattering mechanism could be adjusted through liquid phase sintering,[43] or by expelling secondary phases via phase diagram engineering.[44]

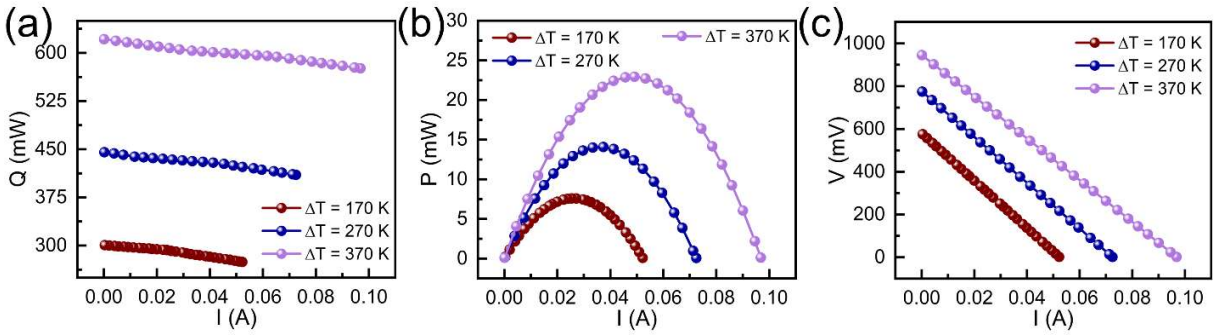

Figure 9 Single leg device measurement results of $Ag_{0.91}Sb_{1.09}Te_{2.09}$ + 0.025 wt% B, showing (a) voltage (V(mV)) vs current (I(A)), (b) Output heat flux (Q(mW)) vs current (I(A)).

Owing to its high average power factor of 1.22 $Wm^{-1}K^{-2}$, $Ag_{0.91}Sb_{1.09}Te_{2.09}$ + 0.025 wt% B demonstrates promising potential for thermoelectric applications. To evaluate this, we fabricated a single-leg device (dimensions: 3mm * 3 mm * 6mm) by densifying powder into a rectangular bar via spark plasma sintering (SPS). During testing, the cold-side temperature (T_c) was maintained at 298 K. As shown in Figure 9a, the maximum heat flux increases from 300.54 mW

at ΔT = 170K to 623.78 mW at ΔT = 370K. Similarly, Figure 9b reveals a rise in power output from 7.58 mW (ΔT = 170K) to 22.86 mW (ΔT = 370K). However, the withdrawn current in these measurements remains below 1 A, which is relatively low.

To investigate this, we analyzed the voltage-current relationship (Figure 9c), which exhibits a linear trend indicative of low internal resistance (R_{int}). The observed low current and high voltage can be attributed to a large load resistance (R_{load}), as per the relation $R_{total} = R_{load} + R_{int} = V/I$. Despite this, the power output ($P = VI$) remains comparable to other $AgSbTe_2$-related systems,[45] underscoring the material's viability. To further enhance performance, optimizing the sample geometry or measurement conditions (e.g., reducing R_{load}) could significantly increase power output.[46]

Conclusion

In summary, this study demonstrates that high-energy ball milling synthesis of $Ag_{0.91}Sb_{1.09}Te_{2.09}$ with 0.025 wt% B significantly enhances the thermoelectric performance of $AgSbTe_2$-based materials, by enhancing the material homogeneity. Unlike conventional annealing-quenching processes, which are energy intensive and potentially hazardous, our synthesis approach enables improved material properties at lower processing temperatures. Structural analyses via X-Ray diffraction (XRD) and scanning electron microscopy (SEM) confirm a notable reduction in Ag_2Te secondary phase formation in the $Ag_{0.91}Sb_{1.09}Te_{2.09}$ + 0.025 wt% B sample. Electrical transport measurements indicate substantial improvements in electrical conductivity and power factor, attributed to increased carrier concentration, enhanced effective mass, improved carrier mobilities (μ_W, μ_H, and μ_0), and a higher intrinsic electronic transport coefficient (σ_{E0}). Notably, the power factor of $Ag_{0.91}Sb_{1.09}Te_{2.09}$ + 0.025 wt% B achieved a high and temperature independent value of 1.22 $Wm^{-1}K^{-2}$, between 300 – 625 K. Simultaneously, thermal conductivity, particularly lattice

thermal conductivity, is markedly suppressed due to the introduction of point defects and dislocations, as supported by the Debye-Callaway model and transmission electron microscopy (TEM) observations.

These synergistic enhancements in electronic transport and thermal resistance lead to a significant improvement in thermoelectric performance. The average figure of merit (zT) increases from 0.56 in pristine $AgSbTe_2$ to 1.03 in $Ag_{0.91}Sb_{1.09}Te_{2.09}$ + 0.025 wt% B, while the peak zT rises from 0.61 to 1.35. Furthermore, single parabolic band (SPB) model suggests that further tuning of the Fermi level and additional reductions in lattice thermal conductivity could potentially elevate the zT up to 1.65. Overall, the combined strategy of boron doping, compositional adjustment, and high-energy ball milling offers a promising route for the development of high-performance thermoelectric materials.

ASSOCIATED CONTENT

AUTHOR INFORMATION

Corresponding Author

Qingyu Yan - School of Materials Science and Engineering, Nanyang Technological University, 50 Nanyang Ave, Block N4.1, Singapore 639798, Republic of Singapore; E-mail: alexyan@ntu.edu.sg

Author Contributions

K.S. carried out experiments and prepared the manuscript. X.Z and Q.Y supervised the project. X.Y.T and M.Z. helped with experiments. Q.Z and P.L carried out HRTEM measurements. Z.L and J.Z carried out device measurements. D.Y helped with Hall measurements. The manuscript

was written through contributions of all authors. All authors have given approval to the final version of the manuscript.

Funding Sources

Q. Yan acknowledges financial support from MOE ACRF Tier 1 RG78/23 and MOE TIER MOE-T2EP50223-0003. X. Wang acknowledges A*STAR RIE 2025 – International Relations Grant Ref Number R24I5IR046. K. Saglik acknowledges the support from A*STAR's SINGA scholarship.

Notes

The authors declare no competing financial interest.

ACKNOWLEDGMENTS

The authors would like to acknowledge the Facility for Analysis, Characterization, Testing and Simulation (FACTS), Nanyang Technological University (NTU), Singapore.

ABBREVIATIONS

AST, $AgSbTe_2$; NS-AST, $Ag_{0.91}Sb_{1.09}Te_{2.09}$

REFERENCES

(1) Jia, N.; Tan, X. Y.; Xu, J.; Yan, Q.; Kanatzidis, M. G. Achieving enhanced thermoelectric performance in multiphase materials. *Accounts of Materials Research* **2022**, *3* (2), 237-246.

(2) Yan, Q.; Kanatzidis, M. G. High-performance thermoelectrics and challenges for practical devices. *Nature materials* **2022**, *21* (5), 503-513.

(3) Snyder, G. J.; Toberer, E. S. Complex thermoelectric materials. *Nature materials* **2008**, *7* (2), 105-114.

(4) Hong, T.; Wang, D.; Qin, B.; Zhang, X.; Chen, Y.; Gao, X.; Zhao, L.-D. Band convergence and nanostructure modulations lead to high thermoelectric performance in $SnPb_{0.04}Te_{-y}\%$ $AgSbTe_2$. *Materials Today Physics* **2021**, *21*, 100505.

(5) Pei, Y.; Wang, H.; Snyder, G. J. Band engineering of thermoelectric materials. *Advanced materials* **2012**, *24* (46), 6125-6135. Park, J.; Xia, Y.; Ozoliņš, V.; Jain, A. Optimal band structure for thermoelectrics with realistic scattering and bands. *npj Computational Materials* **2021**, *7* (1), 43.

(6) Pei, Y.; Gibbs, Z. M.; Gloskovskii, A.; Balke, B.; Zeier, W. G.; Snyder, G. J. Optimum carrier concentration in n-type PbTe thermoelectrics. *Advanced energy materials* **2014**, *4* (13), 1400486.

(7) Zheng, Y.; Slade, T. J.; Hu, L.; Tan, X. Y.; Luo, Y.; Luo, Z.-Z.; Xu, J.; Yan, Q.; Kanatzidis, M. G. Defect engineering in thermoelectric materials: what have we learned? *Chemical Society Reviews* **2021**, *50* (16), 9022-9054.

(8) Dong, J.; Gao, J.; Yan, Q. High entropy strategy on thermoelectric materials. *Materials Lab* **2023**.

(9) Ma, Z.; Luo, Y.; Dong, J.; Liu, Y.; Zhang, D.; Li, W.; Li, C.; Wei, Y.; Jiang, Q.; Li, X. Synergistic Performance of Thermoelectric and Mechanical in Nanotwinned High-Entropy Semiconductors $AgMnGePbSbTe_5$. *Advanced Materials* **2024**, 2407982.

(10) Biswas, K.; He, J.; Blum, I. D.; Wu, C.-I.; Hogan, T. P.; Seidman, D. N.; Dravid, V. P.; Kanatzidis, M. G. High-performance bulk thermoelectrics with all-scale hierarchical architectures. *Nature* **2012**, *489* (7416), 414-418.

(11) Zhou, C.; Lee, Y. K.; Yu, Y.; Byun, S.; Luo, Z.-Z.; Lee, H.; Ge, B.; Lee, Y.-L.; Chen, X.; Lee, J. Y.; et al. Polycrystalline SnSe with a thermoelectric figure of merit greater than the single crystal. *Nature Materials* **2021**, *20* (10), 1378-1384. DOI: 10.1038/s41563-021-01064-6.

(12) Cao, J.; Chien, S. W.; Tan, X. Y.; Tan, C. K. I.; Zhu, Q.; Wu, J.; Wang, X.; Zhao, Y.; Yang, L.; Yan, Q. Realizing *zT* values of 2.0 in cubic GeTe. *ChemNanoMat* **2021**, *7* (4), 476-482.

(13) Witting, I. T.; Chasapis, T. C.; Ricci, F.; Peters, M.; Heinz, N. A.; Hautier, G.; Snyder, G. J. The thermoelectric properties of bismuth telluride. *Advanced Electronic Materials* **2019**, *5* (6), 1800904.

(14) Xu, S.; Liu, Y.; Lee, H.; Li, W. Neural interfaces: Bridging the brain to the world beyond healthcare. *Exploration*, **2024**, 20230146. Chen, Y.; Gao, Z.; Zhang, F.; Wen, Z.; Sun, X. Recent progress in self-powered multifunctional e-skin for advanced applications. *Exploration*, **2022**, 2, 20210112.

(15) Hong, M.; Chen, Z. G.; Yang, L.; Liao, Z. M.; Zou, Y. C.; Chen, Y. H.; Matsumura, S.; Zou, J. Achieving $zT > 2$ in p-type $AgSbTe_{2-x}Se_x$ alloys via exploring the extra light valence band and introducing dense stacking faults. *Advanced Energy Materials* **2018**, *8* (9), 1702333.

(16) Saglik, K.; Dong, J.; Zhang, D.; Hsu, T. Z.; Duran, S. S. F.; Cao, J.; Zhu, Q.; Ji, R.; Kai, W. S.; Lang, T. S. Unlocking the Potential of Cu_3SbSe_3: Ultralow Thermal Conductivity and Enhanced Thermoelectric Performance. *Journal of Solid State Chemistry* **2024**, 124642. Dai, L.; Wang, Z.; Huo, Y.; Huang, Y.; Wang, G.; Fan, L.; Chen, P.; Han, G.; Lu, X.; Zhang, B. Decreased order-disorder transition temperature and enhanced phonon scattering in Ag-alloyed Cu_3SbSe_3. *Journal of Alloys and Compounds* **2022**, *919*, 165829.

(17) Luo, Y.; Du, C.; Liang, Q.; Zheng, Y.; Zhu, B.; Hu, H.; Khor, K. A.; Xu, J.; Yan, Q.; Kanatzidis, M. G. Enhancement of Thermoelectric Performance in $CuSbSe_2$ Nanoplate-Based Pellets by Texture Engineering and Carrier Concentration Optimization. *Small* **2018**, *14* (50), 1803092.

(18) Roychowdhury, S.; Panigrahi, R.; Perumal, S.; Biswas, K. Ultrahigh thermoelectric figure of merit and enhanced mechanical stability of p-type $AgSb_{1-x}Zn_xTe_2$. *ACS Energy Letters* **2017**, *2* (2), 349-356.

(19) Mohanraman, R.; Sankar, R.; Chou, F.; Lee, C.; Chen, Y.-Y. Enhanced thermoelectric performance in Bi-doped p-type $AgSbTe_2$ compounds. *Journal of Applied Physics* **2013**, *114* (16).

(20) Du, R.; Zhang, G.; Hao, M.; Xuan, X.; Peng, P.; Fan, P.; Si, H.; Yang, G.; Wang, C. Enhanced thermoelectric performance of Mg-doped $AgSbTe_2$ by inhibiting the formation of Ag_2Te. *ACS Applied Materials & Interfaces* **2023**, *15* (7), 9508-9516.

(21) Li, K.; Li, Z.; Yang, L.; Xiao, C.; Xie, Y. Charge Compensation Modulation of the Thermoelectric Properties in $AgSbTe_2$ via Mn Amphoteric Doping. *Inorganic Chemistry* **2019**, *58* (14), 9205-9212.

(22) Li, L.; Hu, B.; Liu, Q.; Shi, X. L.; Chen, Z. G. High-Performance $AgSbTe_2$ Thermoelectrics: Advances, Challenges, and Perspectives. *Advanced Materials* **2024**, *36* (45), 2409275.

(23) Ghosh, T.; Roychowdhury, S.; Dutta, M.; Biswas, K. High-performance thermoelectric energy conversion: a tale of atomic ordering in $AgSbTe_2$. *ACS Energy Letters* **2021**, *6* (8), 2825-2837.

(24) Roychowdhury, S.; Ghosh, T.; Arora, R.; Samanta, M.; Xie, L.; Singh, N. K.; Soni, A.; He, J.; Waghmare, U. V.; Biswas, K. Enhanced atomic ordering leads to high thermoelectric performance in $AgSbTe_2$. *Science* **2021**, *371* (6530), 722-727.

(25) Zhang, Y.; Xing, C.; Wang, D.; Genç, A.; Lee, S. H.; Chang, C.; Li, Z.; Zheng, L.; Lim, K. H.; Zhu, H. Realizing high power factor and thermoelectric performance in band engineered $AgSbTe_2$. *Nature communications* **2025**, *16* (1), 22.

(26) Wu, Y.; Liang, Q.; Zhao, X.; Wu, H.; Zi, P.; Tao, Q.; Yu, L.; Su, X.; Wu, J.; Chen, Z. Enhancing thermoelectric performance of $AgSbTe_2$-based compounds via microstructure modulation combining with entropy engineering. *ACS Applied Materials & Interfaces* **2022**, *14* (2), 3057-3065.

(27) Hu, X.; Zheng, S.; Xiong, Q.; Wu, S.; Huang, Y.; Zhang, B.; Wang, W.; Wang, X.; Li, N.; Zhou, Z. Enhancement on thermoelectric performance by Ti doping and vacancies. *Materials Today Physics* **2023**, *38*, 101255.

(28) Cao, J.; Dong, J.; Saglik, K.; Zhang, D.; Solco, S. F. D.; You, I. J. W. J.; Liu, H.; Zhu, Q.; Xu, J.; Wu, J. Non-equilibrium strategy for enhancing thermoelectric properties and improving stability of $AgSbTe_2$. *Nano Energy* **2023**, *107*, 108118.

(29) Gong, Z.; Saglik, K.; Wu, J.; Suwardi, A.; Cao, J. Suppressing Ag_2Te nanoprecipitates for enhancing thermoelectric efficiency of $AgSbTe_2$. *Nanoscale* **2023**, *15* (45), 18283-18290.

(30) Hu, Z.; Yuan, M.; Li, W.; Wang, S.; Li, J.; Jiang, J.; Shuai, J.; Hou, Y. Enhanced thermoelectric performance in pristine $AgSbTe_2$ compound via rational design of Ag2Te formation. *Acta Materialia* **2025**, *290*, 120985.

(31) Saglik, K.; Mete, B.; Terzi, I.; Candolfi, C.; Aydemir, U. Thermoelectric borides: Review and future perspectives. *Advanced Physics Research* **2023**, *2* (8), 2300010.

(32) Wyzga, P.; Wojciechowski, K. Analysis of the influence of thermal treatment on the stability of $Ag_{1-x}Sb_{1+x}Te_{2+x}$ and Se-doped $AgSbTe_2$. *Journal of Electronic Materials* **2016**, *45*, 1548-1554.

(33) Ragimov, S.; Musayev, M.; Hashimova, N. Transport properties of $(AgSbTe_2)_{0.7}(PbTe)_{0.3}$ thermoelectric compound. *Low Temperature Physics* **2022**, *48* (10), 787-790. Wu, H.-j.; Chen, S.-w.; Ikeda, T.; Snyder, G. J. Reduced thermal conductivity in Pb-alloyed $AgSbTe_2$ thermoelectric materials. *Acta Materialia* **2012**, *60* (17), 6144-6151.

(34) Tan, X. Y.; Dong, J.; Liu, J.; Zhang, D.; Solco, S. F. D.; Sağlık, K.; Jia, N.; You, I. J. W. J.; Chien, S. W.; Wang, X. Synergistic Combination of $Sb_2Si_2Te_6$ Additives for Enhanced Average ZT and Single-Leg Device Efficiency of $Bi_{0.4}Sb_{1.6}Te_3$-based Composites. *Advanced Science* **2024**, 2400870. Zhang, Q.; Yuan, M.; Pang, K.; Zhang, Y.; Wang, R.; Tan, X.; Wu, G.; Hu, H.; Wu, J.; Sun, P.; et al. High-Performance Industrial-Grade p-Type $(Bi,Sb)_2Te_3$ Thermoelectric Enabled by a Stepwise Optimization Strategy. *Advanced Materials* **2023**, *35* (21), 2300338. DOI: https://doi.org/10.1002/adma.202300338. Wei, T.-R.; Guan, M.; Yu, J.; Zhu, T.; Chen, L.; Shi, X. How to measure thermoelectric properties reliably. *Joule* 2018, *2* (11), 2183-2188. Borup, K. A.; De Boor, J.; Wang, H.; Drymiotis, F.; Gascoin, F.; Shi, X.; Chen, L.; Fedorov, M. I.; Müller, E.; Iversen, B. B. Measuring thermoelectric transport properties of materials. *Energy & Environmental Science* **2015**, *8* (2), 423-435.

(35) Ma, B.; Ren, H.; Zhang, F.; Peng, Z.; He, H.; Cui, M.; Ge, Z.; Li, B.; Wu, W.; Liang, P. All Cubic-Phase δ-TAGS Thermoelectrics Over the Entire Mid-Temperature Range. *Small* **2023**, *19* (17), 2206439.

(36) Wu, Y.; Qiu, P.; Yu, Y.; Xiong, Y.; Deng, T.; Cojocaru-Mirédin, O.; Wuttig, M.; Shi, X.; Chen, L. High-performance and stable $AgSbTe_2$-based thermoelectric materials for near room temperature applications. *Journal of Materiomics* **2022**, *8* (6), 1095-1103. DOI: https://doi.org/10.1016/j.jmat.2022.07.005.

(37) Zhang, Y.; Li, Z.; Singh, S.; Nozariasbmarz, A.; Li, W.; Genç, A.; Xia, Y.; Zheng, L.; Lee, S. H.; Karan, S. K. Defect-engineering-stabilized $AgSbTe_2$ with high thermoelectric performance. *Advanced Materials* **2023**, *35* (11), 2208994.

(38) Gibbs, Z. M.; Kim, H.-S.; Wang, H.; Snyder, G. J. Band gap estimation from temperature dependent Seebeck measurement—deviations from the $2e|S|_{max}T_{max}$ relation. *Applied Physics Letters* **2015**, *106* (2).

(39) Naithani, H.; Dasgupta, T. Critical analysis of single band modeling of thermoelectric materials. *ACS Applied Energy Materials* **2019**, *3* (3), 2200-2213.

(40) Du, B.; Liu, M.; Xu, J.; Hu, B.; Liu, B.; Su, T.; Wang, J. Thermodynamic, structural and thermoelectric properties of $AgSbTe_2$ thick films developed by melt spinning. *Nanomaterials* **2018**, *8* (7), 474. Jovovic, V.; Heremans, J. Measurements of the energy band gap and valence band structure of $AgSbTe_2$. *Physical Review B—Condensed Matter and Materials Physics* **2008**, *77* (24), 245204.

(41) Li, R.; Han, S.; Zhang, C.; Liu, S.; Yin, W.; Xia, Y.; Liu, P.; Ge, Z.-H.; Zhao, D.; Yang, B.; et al. Supercompliant Lattice Boosts n-type $AgSbTe_2$ Thermoelectrics. *Advanced Functional Materials*, 2502367. DOI: https://doi.org/10.1002/adfm.202502367.

(42) Shuai, J.; Mao, J.; Song, S.; Zhu, Q.; Sun, J.; Wang, Y.; He, R.; Zhou, J.; Chen, G.; Singh, D. J. Tuning the carrier scattering mechanism to effectively improve the thermoelectric properties. *Energy & Environmental Science* **2017**, *10* (3), 799-807.

(43) Zhang, C.; De La Mata, M.; Li, Z.; Belarre, F. J.; Arbiol, J.; Khor, K. A.; Poletti, D.; Zhu, B.; Yan, Q.; Xiong, Q. Enhanced thermoelectric performance of solution-derived bismuth telluride based nanocomposites via liquid-phase Sintering. *Nano Energy* **2016**, *30*, 630-638.

(44) Kim, S. I.; Lee, K. H.; Mun, H. A.; Kim, H. S.; Hwang, S. W.; Roh, J. W.; Yang, D. J.; Shin, W. H.; Li, X. S.; Lee, Y. H. Dense dislocation arrays embedded in grain boundaries for high-performance bulk thermoelectrics. *Science* **2015**, *348* (6230), 109-114.

(45) Chen, B. C.; Wang, K. K.; Wu, H. J. Cation modulation in $AgSbTe_2$ realizes carrier optimization, defect engineering, and a 7% single-leg thermoelectric efficiency. *Small* **2024**, *20* (36), 2401723.

(46) Tan, M.; Liu, W.-D.; Shi, X.-L.; Sun, Q.; Chen, Z.-G. Minimization of the electrical contact resistance in thin-film thermoelectric device. *Applied Physics Reviews* **2023**, *10* (2). DOI: 10.1063/5.0141075